Climate Dynamics (2026) 64:192
https://doi.org/10.1007/s00382-026-08155-7

The influence of soil temperature anomalies in May on high temperature event in June 2023 in North China

Yaoming Song[1,2] · Anning Huang[3] · Haishan Chen[1,2] · Wei Gu[4]

Received: 28 August 2025 / Accepted: 25 February 2026

Abstract
Climate change has led to an increase in the intensity and frequency of extreme high temperature events (HTE). However, there is limited understanding of the impacts of pre-exsiting soil temperature (ST) anomalies on HTEs. Using observations, reanalysis data and numerical experiments, this study investigated the relationships between the May ST in the Huanghuai region and the HTE on June 22 and 23, 2023, in North China. The results show that the ST on May 16 can significantly affect the HTE on June 22 and 23 through its impact on the atmosphere by gravity wave. The ST anomaly persistence can continue to influence the atmosphere and thus modulate subsequent HTE. Propagating from the initial ST anomalies on May 16, subsequent anomalies in the atmosphere, ST and soil moisture affect the HTE on June 22 and 23 in 2023. Through this cascade, the role of the atmospheric anomalies grows progressively more dominant than that of the ST and soil moisture anomalies over time. Moreover, in this individual case, land–atmosphere interactions on June 22 and 23 associated with antecedent ST enhance the HTE, but are not responsible for its occurrence. The conclusions highlight the important role of antecedent ST in HTE, and may draw attention to the important role of antecedent ST in HTE and other extreme events.

Keywords Soil temperature · High temperature event · North China · Persistence

1 Introduction

Global warming leads to the rising of the intensity and frequency of extreme high temperature events (HTE) (Perkins-Kirkpatrick and Lewis 2020; Li et al. 2021; Lesk et al. 2022; IPCC 2023). Extreme HTE has an extensive impact on human health, local ecosystems, social economy (Sun et al. 2014; Zhu et al. 2016; Zhang et al. 2017; Paniw et al. 2022; Lu and Chen 2016; CMA Climate Change Centre 2022). As a densely populated region, North China (NC) (114° E–121° E, 34.5° N–42.5° N) suffered from severe HTE (Ding et al. 2010; Wei and Chen 2011; Wang et al. 2014; Ren et al. 2020).The frequency and intensity of HTE in the NC gradually increased (Wu et al. 2022), and projected heatwave magnitude will increase in NC under the RCP2.6, RCP4.5, and RCP8.5 scenarios (Xu et al. 2024). From mid-June through early July 2023, an extreme HTE occurred in NC (Xiao et al. 2024). The number of high temperature (daily maximum temperature≥35 °C) days in NC reached 9.8 days in June, which was the fourth most in the same period in history since 1961 (http://news.weather.com.cn/2023/06/3632314.shtml). From June 21 to 30 in 2023, the daily maximum temperature exceeded 40 °C at 124 observation stations in NC (http://news.weather.com.cn/2023/07/3632644.shtml).

Both numerical simulations and diagnostic analyses show that antecedent sea surface temperature, soil moisture (SM) and concurrent synoptic circulation patterns have an

✉ Yaoming Song
songym@nuist.edu.cn

1 State Key Laboratory of Climate System Prediction and Risk Management/Key Laboratory of Meteorological Disaster, Ministry of Education/Collaborative Innovation Center On Forecast and Evaluation of Meteorological Disasters, Nanjing University of Information Science and Technology, Nanjing 210044, China

2 School of Atmospheric Sciences, Nanjing University of Information Science and Technology, Nanjing, Jiangsu, China

3 School of Atmospheric Sciences, Nanjing University, Nanjing, China

4 Laboratory for Climate Studies, National Climate Center, China Meteorological Administration, Beijing 100081, China

Published online: 07 April 2026

important influence on the HTE in NC. The HTE in NC is related to climate change, anthropogenic activity, land-surface interaction and atmospheric circulation (Wu et al. 2021). The sea surface temperature over the Northwest Pacific during April–May, the sea surface temperature tendency over the North Atlantic and the central-eastern Pacific from April to May, the 2-m temperature warming tendency from December-January to April–May over Russia are the important predictability sources of extreme high temperature days in NC (Li and Ye 2024). Soil moisture in spring or early summer is also closely linked to summer THE in NC (Wu and Zhang 2015; Zhang et al. 2015). Moreover, synoptic circulation patterns play a key role in regional dry and moist heat waves in NC (An and Zuo 2021), and the severe HTE over NC in late June 2023 is accompanied by anomalous anticyclone (Wang et al. 2024; Xiao et al. 2024). Compared to current climate conditions, extreme three-day HTE in NC in late June 2023 are projected to increase in both frequency and intensity in future (Qian et al. 2024).

As a critical parameter characterizing soil thermal status and land–atmosphere interactions, the effect of antecedent soil temperature (ST) on atmosphere, especially its contribution to extreme heat events, remains inadequately studied. Due to the memeory of soil thermal anomalies, to what extent can antecedent ST influence HTE? Numerical experiments demonstrated that the deep ST on the previous day can produce a meaningful impact on the HTE (Gómez et al. 2016). In terms of climatological characterization of HTE, spring ST over central Asia may lead to more HTE in summer via the effects on geopotential height anoamlies (Yang et al. 2019). However, the potential influence of antecedent ST with lead times of weeks to months on a given THE remains poorly understood, and this study focuses on whether antecedent ST can influence the extreme HTE in late June 2023 in NC.

2 Methodology

2.1 Data and statistical analysis

Daily maximum, minimum and average temperature observation data at 2 m in 2023 are from National Centers for Environmental Information (https://www.ncei.noaa.gov/maps/daily) and the site number in China is 408. Monthly skin temperature (TSK) observation data at 1085 sites from 1960 to 2013 is provided by the China Meteorological Administration (http://data.cma.cn/data/detail/dataCode/A.0053.0002.S004.html). ERA5-Land maximum air temperature at 2 m (Tmax) and ST daily data of four soil levels (0–7, 7–28, 28–100, and 100–289 cm) in 2023 were used. Monthly ERA5-land ST data at the four soil levels and air temperature at 2 m (T2m) from 1979 to 2023 were used. The horizontal resolution of ERA5-land data is 0.1° × 0.1°. The daily Tmax observations are obtained from the China Meteorological Administration (http://data.cma.cn/data/detail/dataCode/A.0012.0001.html), which spans the period from 1951 to 2024.

To understand the antecedent ST signals associated with the June Tmax, Pearson correlation coefficient was used to analyze the relationships between the observed June Tmax and the ERA5-Land ST in both June and the preceding May. The analysis utilized data spanning the period from 1979 to 2022.

2.2 Numerical experimental design

The numerical experiments were performed using the Weather Research and Forecasting (WRF) model (Skamarock et al. 2008), and the version is 4.3. The simulation domain is centered at (35° N, 100° E), and the total grid points is 80 (west–east) × 50 (south–north), with the horizontal grid spacing is 100 km. Initial and boundary conditions are provided by NCEP-FNL.

The control experiment (CTL) was performed starting from May 15th to June 30th. In sensitivity experiments, the area where ST anomalies were filled is from 110° E to 121° E and from 30° N to 40° N. This key region was identified based on the relationship (Sect. 3.2) between the June Tmax and the ST in both June and May using ERA5-Land data. The added ST anomalies were referenced to the standard deviation of the observed skin temperature (TSK) in May from 1960 to 2019 (Fig. 1). Given the global warming trend, positive ST anomalies were incorporated into the initial ST conditions of the CTL. Five sensitivity experiments (SEN, JUN1-STSM, JUN1-ST, JUN20-STSM, JUN20-ST) were conducted, starting from May 16, June 1, June 1, June 20 and June 20, respectively. The atmospheric and soil conditions simulated by CTL at 0:00 on May 16th was used as the initial condition of SEN after adding ST anomalies. The initial atmospheric state for JUN1-STSM was taken directly from the SEN run at 00:00 on June 1. The initial soil state for JUN1-STSM was constructed by taking the SEN state at 00:00 on June 1 and replacing its ST and SM fields with the values from the CTL run at the corresponding time. In JUN1-ST, the initial atmospheric condition was the same as the one simulated by SEN at 0:00 on June 1, and the soil condition simulated by SEN at 0:00 on June 1 was used as the initial soil condition of JUN1-ST after the ST in it were replaced by the one at the corresponding time in CTL. Experimental details are provided in Table 1. The experimental design of JUN20-STSM and JUN20-ST were similar to those of JUN1-STSM and JUN1-ST (Table 1). The two groups of experiments were designed to test the subsequent

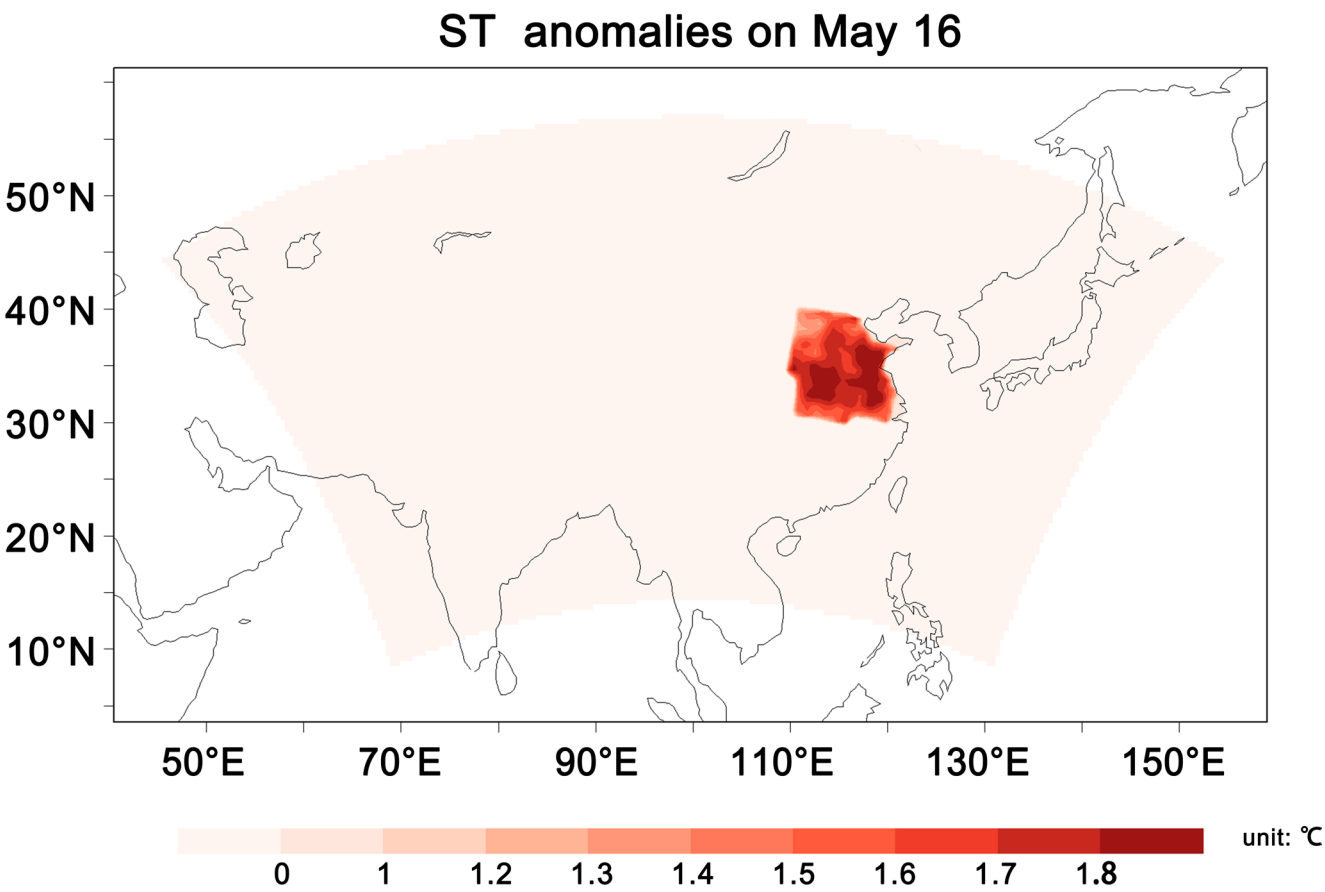

Fig. 1 ST anomalies used to initialize the SEN experiment, which were referenced to the standard deviation of TSK in May from 1960 to 2019. The shaded region corresponds to the model domain

Table 1 Schemes of the numerical experiments

The 'Initial condition' column indicates that the model was initialized using the atmospheric and land surface states from the CTL or SEN experiment at the corresponding time listed in the 'Initialization time' column

Experiment	Initial condition			Initialization time	Lateral boundary
	Atmosphere	ST	SM		
CTL	NCEP-FNL	NCEP-FNL	NCEP-FNL	May 15th	NCEP-FNL
SEN	CTL	CTL + ST anomalies	CTL	May 16th	NCEP-FNL
JUN1-STSM	SEN	CTL	CTL	June 1st	NCEP-FNL
JUN1-ST	SEN	CTL	SEN	June 1st	NCEP-FNL
JUN20-STSM	SEN	CTL	CTL	June 20th	NCEP-FNL
JUN20-ST	SEN	CTL	SEN	June 20th	NCEP-FNL

Table 2 Calculation design for the separate impact of ST, SM and atmospheric anomalies on June 1 (originating from the ST anomalies on May 16) on subsequent states of atmosphere and land surface

Experiment	Separate impact
SEN – CTL	Initial ST anomalies on May 16
JUN1-STSM – CTL	Atmospheric anomalies on June 1 caused by ST anomalies on May 16
SEN – JUN1-ST	ST anomalies on June 1 caused by ST anomalies on May 16
JUN1-ST – JUN1-STSM	SM anomalies on June 1 caused by ST anomalies on May 16

atmospheric and land-surface responses after separately removing the ST, SM, and atmospheric anomalies on June 1 and June 20, respectively. And these anomalies were induced by the May 16 ST event. The ultimate objective is to determine whether the impact of the May 16 ST anomalies on the HTE on June 22 and 23 is mediated primarily through the atmospheric pathway, the ST and SM pathway, or both.

As shown in Table 2, the differences between SEN and CTL were used to estimate the influence of the initial ST on May 15 on the subsequent atmosphere and land surface. The differences between SEN and JUN1-STSM were used to estimate the response of the atmosphere and land surface to the June 1 ST and SM anomalies (originating from the May 16 ST anomalies), with the June 1 atmospheric anomalies

caused by the May 16 ST anomalies removed. The differences between SEN and JUN1-ST were used to estimate the response of the atmosphere and land surface to the June 1 ST anomalies caused by the May 16 ST anomalies, with the June 1 atmospheric and SM anomalies attributable to the May 16 ST anomalies removed. The differences between JUN1-STSM and CTL were used to estimate the response of the atmosphere and land surface to June 1 atmospheric anomalies originating from the May 16 ST anomalies, with the June 1 ST and SM anomalies caused by the May 16 ST anomalies removed. The differences between JUN1-ST and JUN1-STSM represent the separate response of the atmospheric and land surface to the June 1 SM anomalies originating from the May 16 ST anomalies. Similar assessments were also conducted on June 20 using the differences among SEN, JUN20-STSM and JUN20-ST.

3 Results

3.1 The characteristics of the HTE in observation, ERA5-land and simulations

Figure 2 shows there is an extreme HTE in NC on Jun 22 and 23 in 2023, and Tmax exceeds 40 °C in some areas of NC (Xiao et. al., 2024). The spatial distribution of the Tmax of ERA5-Land is in good agreement with observation in NC (Fig. 2a, b). The Tmax on June 22 and 23 simulated by CTL shows similar spatial characteristics to observation, but the area with Tmax above 34 °C is smaller, and the simulated Tmax is lower in the eastern and northern parts of NC (Shandong, Liaoning and the northern part of Jiangsu). The CTL simulation can reproduce the high temperature in Mongolia, India, Northwest China and NC (Fig. 2c). Moreover, the spatial distribution of Tmax simulated by the SEN experiment is also similar to that of the CTL experiment, but the Tmax is considerably higher in the Huanghuai region (approximately 110°–121° E, 30°–40° N) (Fig. 2d). The significant positive and negative Tmax anomalies induced by the initial ST anomalies are located in the Huanghuai region and northeastern China, respectively (Fig. 2e).

3.2 The statistical relationship between antecedent ST and the near surface temperature in June

The relationships between antecedent ST and the near surface temperature in June are represented by the correlation coefficients between the air temperature at 2 m in June and the ST at the four soil levels in May and June from 1979 to 2022. In June, the correlation decreases with increasing soil depth (Fig. 3a–d). Meanwhile, there was a statistically significant linear relationship between ST in May in the Huanghuai region and the June T2m in NC (Fig. 3e–h). Moreover, the area with high correlation shifts from the top three soil levels in NC to the four soil levels in the Huanghuai region, and the May ST in the Huanghai region is closely related to the June T2m in NC. In May, the correlation in the third soil level is greater than one in the first and second soil levels. Therefore, the May ST may have some physical connection with the June T2m, and then may alter the HTE in June through atmospheric and soil conditions associated with the T2m.

3.3 The influence of antecedent ST on the Tmax on Jun 22 and 23 in 2023

The positive ST anomalies on May 16 lead to the obvious positive and negative Tmax anomalies in the Huanghuai region and northeastern China on June 22 and 23 in 2023, respectively, and the absolute value of the anomalies can reach about 5 °C in some areas (Fig. 4a). The positive Tmax anomalies in the Huanghuai region imply an enhancement

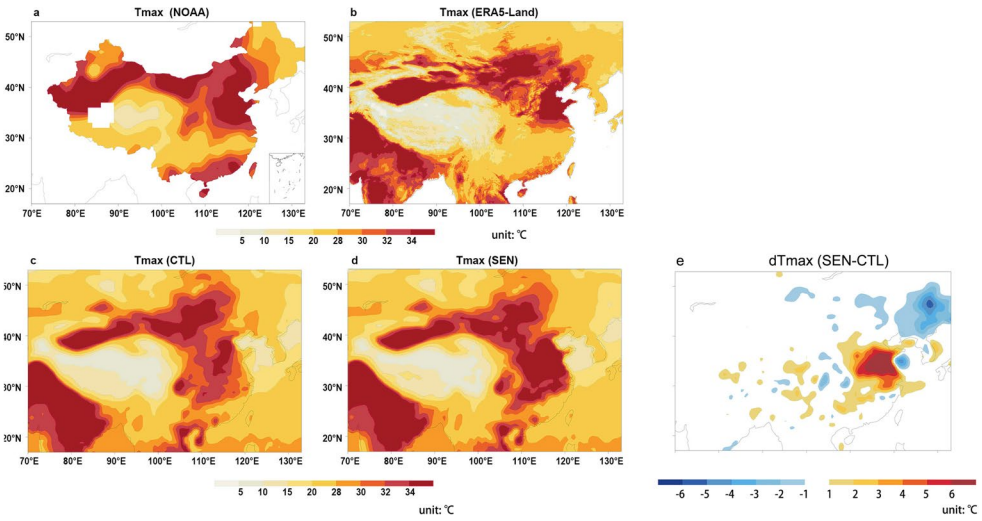

Fig. 2 The spatial distributions of the Tmax on June 22 and 23. **a** is the observed Tmax. **b** The Tmax in ERA5-Land. **c** The simulated Tmax in CTL experiment using WRF. **d** The simulated Tmax in SEN experiment using WRF. **e** The simulated Tmax anomalies (SEN-CTL)

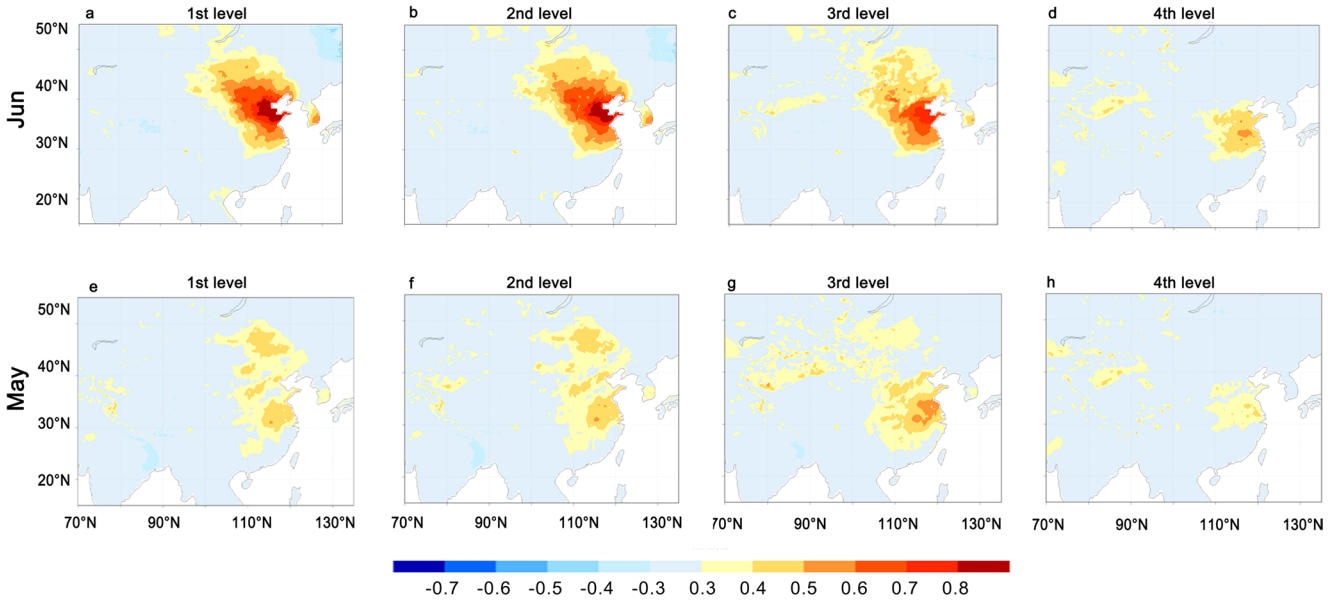

Fig. 3 The correlation coefficients between the Tmax in June and antecedent ST (1979–2022). **a**, **b**, **c** and **d** correspond to the 1st, 2nd, 3rd and 4th soil layers in June, respectively. **e**, **f**, **g** and **h** correspond to the 1st, 2nd, 3rd and 4th soil layers in May, respectively. The warm-colored shaded areas represent the 95% confidence level using the T test

of HTE in the southern part of NC, and this enhancement is caused by the initial positive ST anomalies.

After removing the June 1 ST and SM anomalies that originated from the May 16 ST anomalies, the remaining atmospheric anomalies on June 1, which are also induced by May 16 ST anomalies, can still generate a spatial pattern of Tmax anomalies similar to that in Fig. 4b,though the anomalies are weaker in magnitude.

Moreover, as shown in Fig. 4c and d, after removing the atmospheric anomaly signals on June 1 caused by the May 16 ST anomalies, the June 1 ST and SM anomalies caused by the May 16 ST anomalies can still produce the Tmax anomalies that are spatially similar to those in Fig. 4b. Additionally, these Tmax anomalies are stronger than those in Fig. 4a in northeastern China. Furthermore, the separate impact of the June 1 SM anomalies is opposite to that of the June 1 ST anomalies. While positive ST anomalies lead to higher T2m, positive SM anomalies result in decreased T2m. In other words, the atmospheric, ST and SM anomalies on June 1 caused by the ST anomalies on May 16 can all play an important role in the connection between the ST anomalies on May 16 and the Tmax anomalies on June 22 and 23.

Furthermore, the atmospheric anomalies on June 20, which caused by the ST anomalies on May 16, are capable of producing the Tmax anomalies on June 22 and 23 similar to those in Fig. 4e, both in spatial extent and degree of anomaly. However, the ST and SM anomalies on June 20, which caused by the ST anomalies on May 16, have little effect on the Tmax anomalies on June 22 and 23 (Fig. 4f and g). In other words, the June 20 atmospheric anomalies caused by the May 16 ST anomalies mainly determine the connection between the May 16 ST anomalies and the Tmax anomalies in Fig. 4a. In contrast, the contributions from the June 20 ST and SM anomalies caused by the May 16 ST anomalies are negligible (Fig. 4f and g).

In summary, the ST anomalies on May 16 lead to subsequent ST and SM anomalies, and the persistence of the anomalies in soil can continuously affect the atmosphere. On June 20, the ST and SM anomalies are no longer important in the connection between the May 16 ST anomalies and the Tmax anomalies in Fig. 4a. In other words, the concurrrent local land–atmosphere interaction is not responsible for the occurrence of the Tmax anomalies in Fig. 4a.

3.4 The physical processes related to the influence of antecedent ST on the HTE in June

The initial ST anomalies can subsequently induce anomalies in ST, SM and the atmosphere. The ST anomalies originating on May 15 propagate downward over time and can persist through June. In the deep soil layers, these anomalies can maintain a magnitude of no less than 0.4 °C (Fig. 5a). The negative ST anomalies correspond to the positive SM anomalies (Fig. 5a and b). The positive SM anomalies are attributable to precipitation anomalies, which are caused by atmospheric anomalies originating from the May 16 ST anomalies. Moreover, the impact of the May 16 ST anomalies on subsequent ST is more pronounced than their impact on subsequent SM. The separate impact of ST and

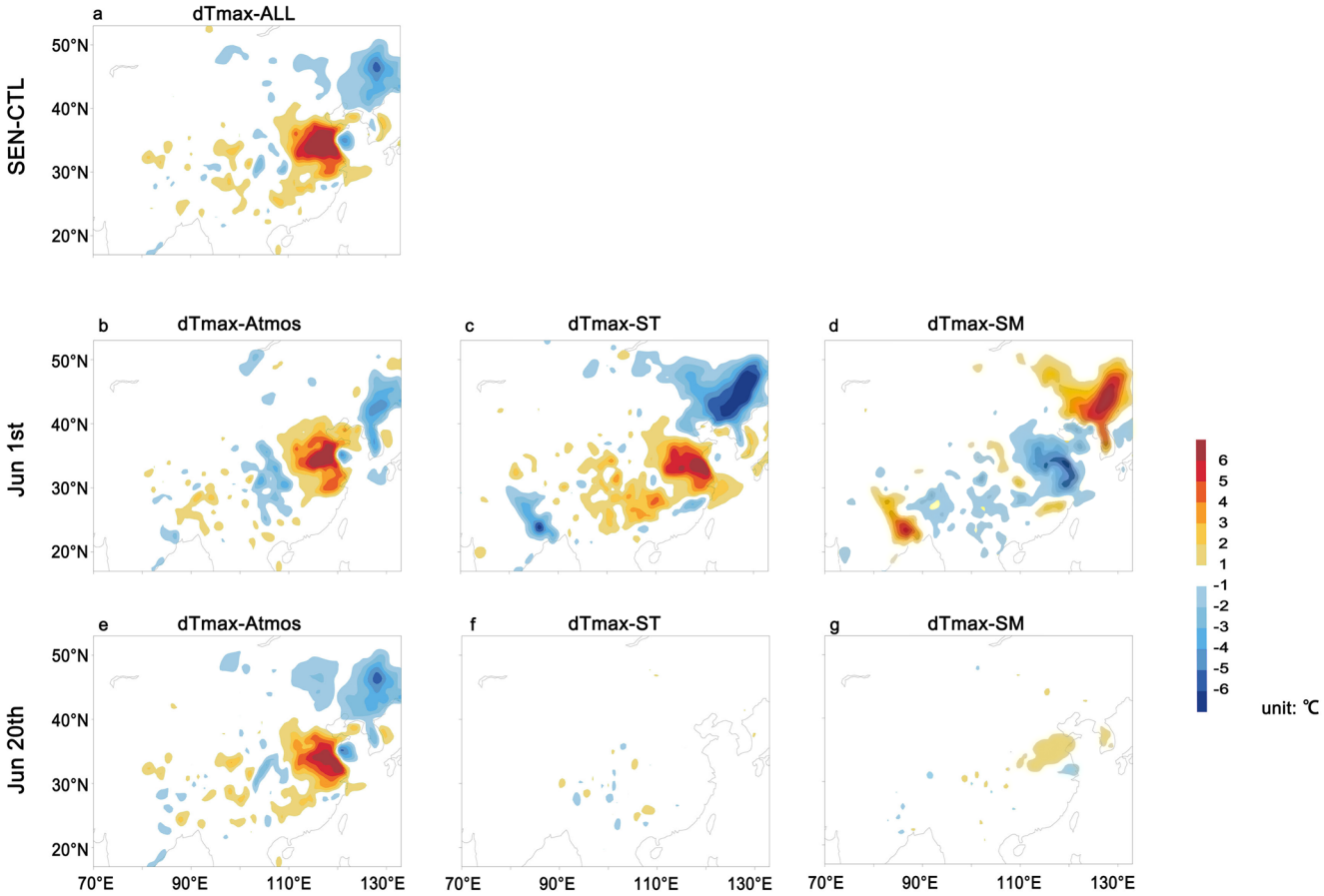

Fig. 4 The Tmax anomalies on June 22 and 23 caused by ST, SM and atmosphere anomalies. **a** The Tmax anomalies caused by the May 16 ST anomalies (SEN minus CTL). **b** The Tmax anomalies caused by the June 1 atmosphere anomalies (JUN1-STSM minus CTL). **c** The Tmax anomalies caused by the June 1 ST anomalies (SEN minus JUN1-ST). **d** The Tmax anomalies caused by the June 1 SM anomalies (JUN1-ST minus JUN1-STSM). **e** The Tmax anomalies caused by the atmosphere anomalies on June 20 (JUN20-STSM minus CTL). **f** The Tmax anomalies caused by the ST anomalies on June 20 (SEN minus JUN20-ST). **g** The Tmax anomalies caused by the SM anomalies on June 20 (JUN20-ST minus JUN20-STSM)

atmospheric anomalies originating from the May 16 ST anomalies on the ST condition on June 22 and 23 show the similar characteristics to the impact from the May 16 ST anomalies. The positive ST anomalies in late June originated from the atmospheric anomalies induced by the positive ST anomalies on May 16. The May 16 ST anomalies propagated through subsequent atmospheric, ST, and SM anomalies, ultimately leading to the atmospheric anomalies in late June. Moreover, the SM anomalies induced by the May 16 ST anomalies can generate the negative ST anomalies and positive SM anomalies on June 22 and 23, consequently resulting in negative Tmax anomalies on June 22 and 23 (Fig. 5g and h). The separate impacts of the June 20 and June 1 anomalies in ST, SM and atmosphere are similar, with both sets stemming from the May 16 ST anomalies (Fig. S1).

The persistence of ST and SM anomalies in soil can affect subsequent atmosphere. The May 16 ST anomalies in the Huanghuai region lead to a significant increase in spatially averaged atmospheric anomalies and land–atmosphere flux anomalies in the simulation domain over time (Fig. 6). From mid-June, the atmospheric temperature anomalies can reach the order of 10^{-1} °C, while the geopotential anomalies can reach the order of 101 m^2/s^2 (Fig. 6a). Moreover, the anomalies of heat fluxes and radiation fluxes can reach the order of 102 W/m^2 after about June 10 (Fig. 6b). The response of atmosphere to ST anomalies is controlled by atmospheric thermodynamics and dynamical equations. Following the introduction of the positive ST anomalies into the Huanghuai region, ST anomalies trigger a rapid atmospheric response through the excitation of gravity waves (Fig. 7). By one hour after initiation, the region significantly affected by gravity waves covers the area within 25°–42° N and 100°–130° E; by the sixth hour, it has expanded to include Bangladesh and the South China Sea (Fig. 7). The atmospheric anomalies undergo sustained growth, driven by persistent land surface anomalies originating from the May 16 ST anomalies (Figs. 5 and 6). And the persistent forcing from

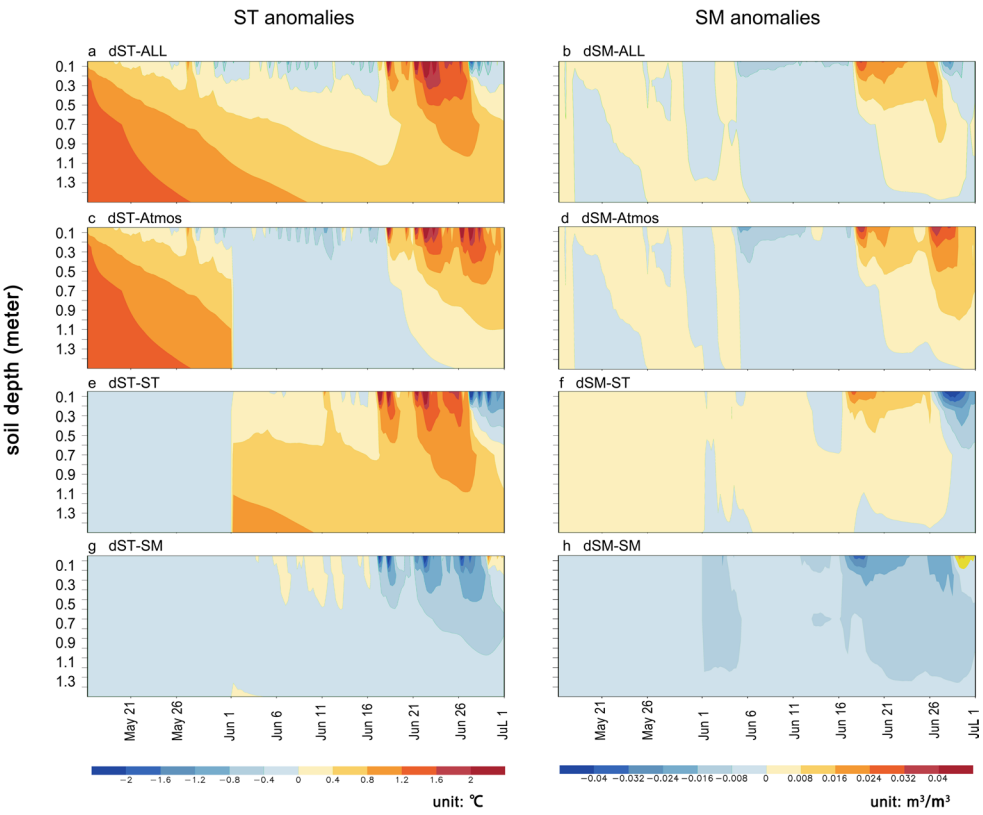

Fig. 5 Spatially averaged ST and SM anomalies induced by the June 1 anomalies, which were initiated by the May 16 ST anomalies. The first and second columns correspond to ST and SM anomalies, respectively. **a** and **b** represent the ST and SM anomalies caused by the May 16 ST anomalies (SEN minus CTL), respectively. **c** and **d** denote the ST and SM anomalies caused by the June 1 atmosphere anomalies (JUN1-STSM minus CTL), respectively. **e** and **f** are the ST and SM anomalies caused by the June 1 ST anomalies (SEN minus JUN1-ST), respectively. **g** and **h** correspond to the ST and SM anomalies caused by the June 1 SM anomalies (JUN1-ST minus JUN1-STSM), respectively

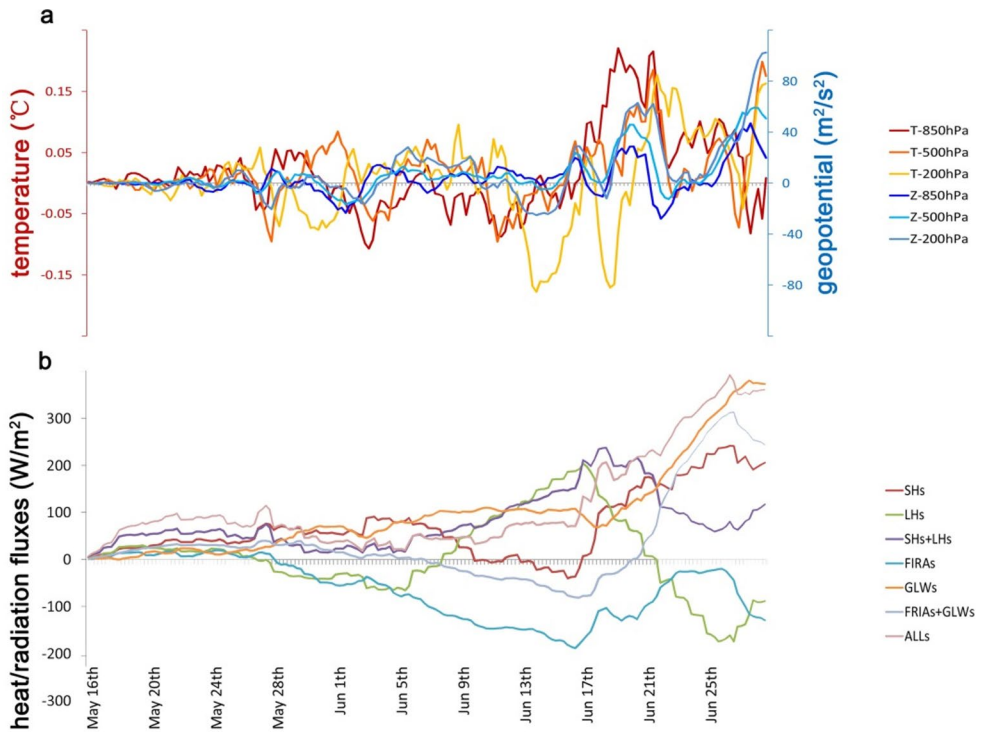

Fig. 6 Spatially averaged atmospheric anomalies and land–atmosphere flux anomalies caused by the positive ST anomalies on May 16 (SEN – CTL). **a** The changes of air temperature and geopotential anomalies over time. **b** The changes of heat and radiation flux anomalies over time. T-850 hPa, T-500 hPa and T-200 hPa represent the spatially averaged air temperature of 850 hPa, 500 hPa and 200 hPa, respectively. Z-850 hPa, Z-500 hPa and Z-200 hPa represent geopotential of 850 hPa, 500 hPa and 200 hPa, respectively. SHs, LHs, FIRAs, GLWs correspond to the spatially averaged sensible heat flux (SH), latent heat flux, net longwave radiation and downward longwave radiation at ground surface, respectively. ALLs represent the sum of SHs, LHs, FIRAs and GLWs

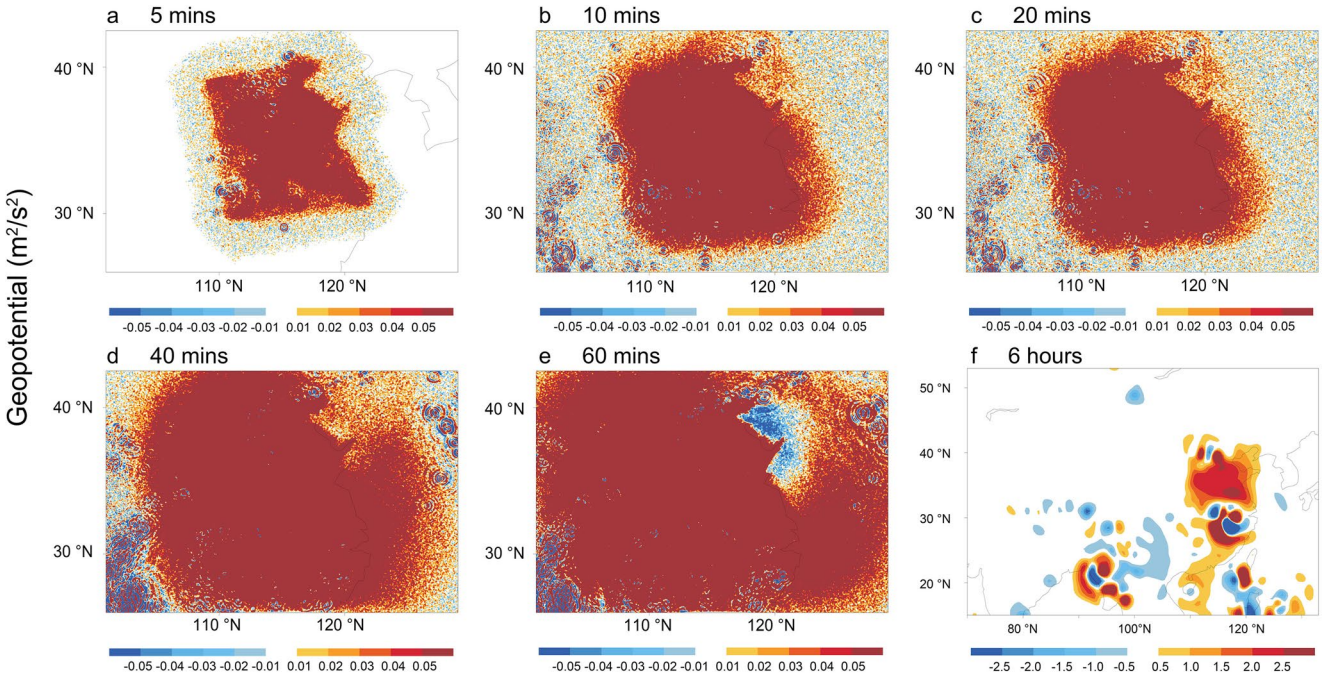

Fig. 7 The geopotential anomalies caused by positive ST anomalies at 0:00 on May 16 (SEN—CTL). The geopotential anomalies of 850 hPa after 5 min (**a**), 10 min (**b**), 20 min (**c**), 40 min (**d**) and 60 min (**e**). **f** is the geopotential anomalies of 500 hPa after 6 h

the land surface anomalies caused by the May ST anomalies leads to continuous adjustments in atmospheric wind speed, geopotential height and other atmospheric variables (Fig. 8). The impacted area is not limited to North China and the Huang-Huai region, with distinct atmospheric anomalies also present in other regions (Fig. 8).

$$\frac{\partial T}{\partial t} = -V_h \cdot \nabla_h T - \omega \frac{\partial T}{\partial p} + \frac{RT}{c_p p}\omega + \frac{\dot{Q}}{c_p} \quad (1)$$

where T and t are air temperature and time, respectively; V_h and ω are the horizontal and vertical velocities in the pressure coordinate, respectively; $\dot{Q}$ represents nonadiabatic heating, such as heat and radiation fluxes; p is air pressure, solar radiation reflected by land surface, thermal radiation emitted by land surface, sensible and latent heat fluxes, respectively; R and c_p are specific heat capacity at constant pressure and dry air specific gas constant, respectively.

Following the fundamental atmospheric temperature tendency equation derived from the first law of thermodynamics (Eq. 1), the continuously enhanced atmospheric anomalies lead to the Tmax anomalies on June 22 and 23, and the Tmax anomalies were enhanced through land–atmosphere interactions (Fig. 9). The anomalies of atmospheric temperature and circulation produce warm and cold advection (Fig. 9f), which contributes to the warm and cold atmospheric internal energy anomalies in Huanghuai and northeastern China, respectively (Fig. 9e). The warm atmospheric internal energy anomalies lead to positive downward longwave radiation anomalies in Huanghuai (Fig. 9c), which increases skin temperature (TSK) in Huanghuai (Fig. 9h). The increased TSK then makes T2m increases through the increased SH in Huanghuai (Fig. 9a), while the opposite is true in northeastern China (Fig. 9a). Moreover, horizontal heat transport near the land surface also contributes to the near-surface temperature anomalies (Fig. 9b). There are not significant downward solar radiation anomalies in Huanghuai, which implies that downward solar radiation is not responsible for the Tmax anomalies on June 22 and 23 (Fig. 9i). Meanwhile, the increased TSK enhances upward longwave radiation, further warming the atmosphere in Huanghuai (Fig. 9d). In summary, both temperature advection anomalies and SH anomalies play a crucial role in the Tmax anomalies in Fig. 4a.

4 Conclusion and discussion

Monthly temperature anomalies provide a backdrop for daily extreme events (Yang et al. 2019; Hoogewind et al. 2025). Using ERA5-Land data and observations, we found that the T2m in June in NC is significantly related to the May ST in the Huanghuai region, suggesting their potential monthly-scale connection. Numerical simulations confirm that the positive May 16 ST anomalies in the Huanghuai region can lead to the positive Tmax anomalies in the southern part of NC, and the anomalies can reach about 5 °C in

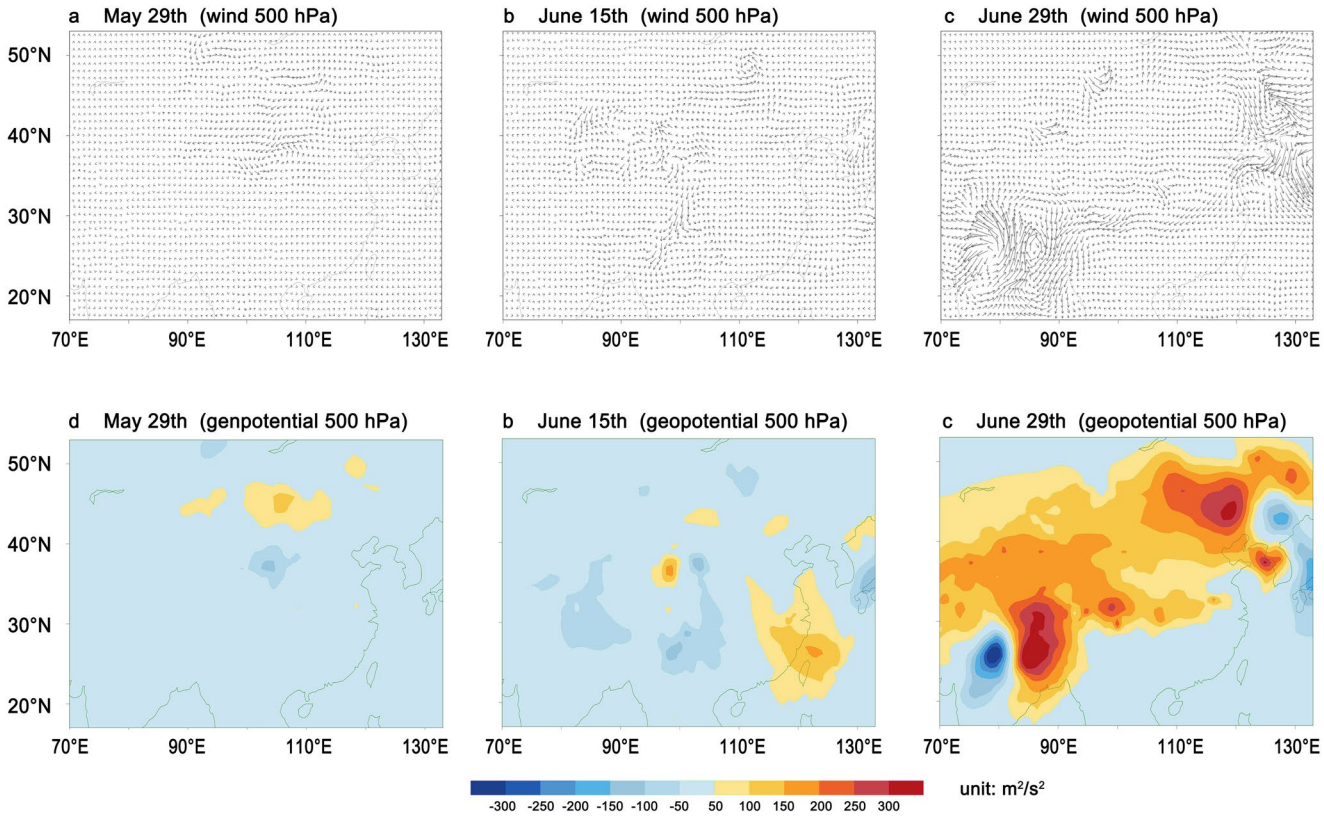

Fig. 8 The anomalies of wind and geopotential caused by the positive ST anomalies on May 16 (SEN – CTL). **a**, **b** and **c** correspond to the wind of 500 hPa on May 29, on June 15 and on June 29, respectively. **d**, **e** and **f** correspond to the geopotential of 500 hPa on May 29, on June 15 and on June 29, respectively

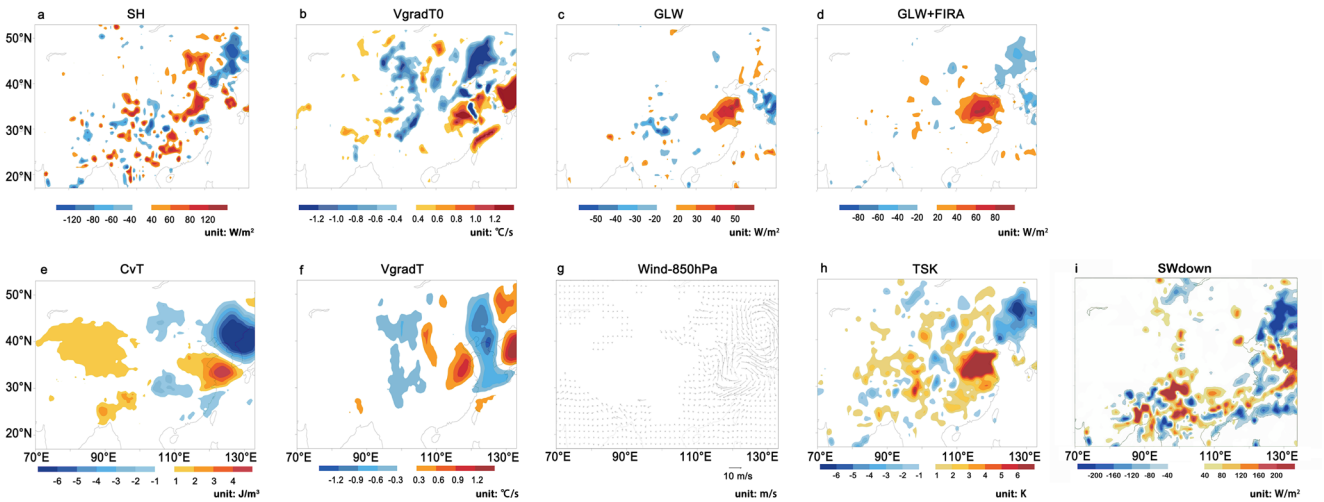

Fig. 9 The anomalies of atmosphere and land surface fluxes on June 22 and 23 caused by the positive ST anomalies on May 16 (SEN – CTL). **a** SH. **b** temperature advection at ground surface (VgradT0). **c** downward longwave radiation at ground surface (GLW). **d** upward longwave radiation at ground surface (GLW+FIRA). **e** The vertical integral of the internal energy of the atmosphere (CvT). **f** The vertical integral of temperature advection of the atmosphere (VgradT). **g** The wind of 850 hPa (Wind-850 hPa). **h** The skin temperature (TSK). (i) The downward solar radiation (SWdown)

some areas, which modulates the HTE in NC on June 22 and 23.

The May 16 ST anomalies lead to subsequent ST and SM anomalies, and then continuously affect local and remote atmosphere, with gravity waves being an important way. Driven by persistent land surface anomalies, atmospheric anomalies amplify over time. And then, the atmospheric anomalies determine the influence of the May 16 ST on the Tmax on June 22 and 23 through temperature advection anomalies. While not responsible for the occurrence of the Tmax anomalies on June 22 and 23, the land–atmosphere interactions on June 22 and 23 contributed to their intensification. Temperature advection anomalies lead to warm and cold atmospheric temperature anomalies in the southern part of NC and northeastern China, respectively. In NC, warmer atmospheric temperature increases downward longwave radiation, leading to increased TSK. The anomalies of TSK cause the T2m anomalies through SH. And the anomalies of upward longwave radiation caused by the TSK anomalies can lead to the atmospheric anomalies, which can affect the downward longwave radiation.

Previous studies indicate that HTE may be influenced by the ST of previous day, and that the climatological characterization of HTE in summer may be affected by spring ST. However, the potential influence of ST from days to even a month prior on a given HTE remains unclear. This study confirmed that ST has an important impact on the HTE one month later through the atmosphere anomalies due to the persistence of soil anomalies. Moreover, the anomalies in ST and SM from the preceding day show a minimal effect on the HTE in this study. Additionally, gravity wave is an important way for ST to affect remote atmosphere. Understanding the antecedent signals and physical processes associated with HTE provides deeper insight into their formation mechanisms. Our findings highlight the critical role of ST in subsequent extreme events.

Supplementary Information The online version contains supplementary material available at https://doi.org/10.1007/s00382-026-08155-7.

Acknowledgements This work was supported by the National Natural Science Foundation of China (Grant Nos. 42130609, 41975081 and 41005047).

Data availability Daily temperature observation data at 2 m is available at https://www.ncei.noaa.gov/maps/daily. ERA5-Land data is available at https://cds.climate.copernicus.eu/datasets/derived-era5-land-daily-statistics?tab=download. The daily skin temperature and maximum air temperature at 2 m data can be obtained from the China Meteorological Administration (http://data.cma.cn/data/).

Declarations

Conflict of interest The authors have no relevant financial or non-financial interests to disclose.

References

An N, Zuo Z (2021) Investigating the influence of synoptic circulation patterns on regional dry and moist heat waves in North China. Clim Dyn 57(3):1227–1240. https://doi.org/10.1007/s00382-021-05769-x

CMA Climate Change Centre (2022) Blue Book on Climate Change in China (2022). Science Press, Beijing, p 109

Ding T, Qian W, Yan Z (2010) Changes in hot days and heat waves in China during 1961–2007. Int J Climatol 30(10):1452–1462. https://doi.org/10.3724/SP.J.1248.2014.066

Gómez I, Caselles V, Estrela MJ, Niclòs R (2016) Impact of initial soil temperature derived from remote sensing and numerical weather prediction datasets on the simulation of extreme heat events. Remote Sens 8(7):589. https://doi.org/10.3390/RS8070589

Hoogewind KA, Gensini VA, Brooks HE (2025) On the relationship between monthly mean surface temperature and tornado days in the United States. Npj Climate and Atmospheric Science 8(1):119. https://doi.org/10.1038/s41612-025-00993-2

IPCC (2023) Climate change 2021: The physical science basis. Cambridge University Press., 2392 pp. https://doi.org/10.1017/9781009157896

Lesk C, Anderson W, Rigden A, Coast O, Jägermeyr J, McDermid S et al (2022) Compound heat and moisture extreme impacts on global crop yields under climate change. Nat Rev Earth Environ 3:872–889. https://doi.org/10.1038/s43017-022-00368-8

Li J, Ye L (2024) Predictability of the anomaly pattern of summer extreme high temperature days over northern China. Clim Dyn 62:7687–7700. https://doi.org/10.1007/s00382-024-07301-3

Li C, Zwiers F, Zhang X, Li G, Sun Y, Wehner M (2021) Changes in annual extremes of daily temperature and precipitation in CMIP6 models. J Climate 34:3441–3460. https://doi.org/10.1175/JCLI-D-19-1013.1

Lu R, Chen R (2016) A review of recent studies on extreme heat in China. Atmos Oceanic Sci Lett 9:114–121. https://doi.org/10.1080/16742834.2016.1133071

Paniw M, Duncan C, Groenewoud F, Drewe JA, Manser M, Ozgul A, Clutton-Brock T (2022) Higher temperature extremes exacerbate negative disease effects in a social mammal. Nat Clim Chang 12:284–290. https://doi.org/10.1038/s41558-022-01284-x

Perkins-Kirkpatrick SE, Lewis SC (2020) Increasing trends in regional heatwaves. Nat Commun 11:3357. https://doi.org/10.1038/s41467-020-16970-7

Qian C, Ye Y, Jiang J, Zhong Y, Zhang Y, Pinto I et al (2024) Rapid attribution of the record-breaking heatwave event in North China in June 2023 and future risks. Environ Res Lett 19(1):014028. https://doi.org/10.1002/joc.857

Ren L, Zhou T, Zhang W (2020) Attribution of the record-breaking heat event over Northeast Asia in summer 2018: the role of circulation. Environ Res Lett 15(5):054018. https://doi.org/10.1088/1748-9326/ab8032

Skamarock WC, Klemp JB, Dudhia J, Gill DO, Barker DM, Duda MG, et al (2008) A description of the Advanced Research WRF version 3. NCAR Tech. Note NCAR/TN-4751STR, 113 pp. https://doi.org/10.5065/D68S4MVH

Sun Y, Zhang X, Zwiers F, Song L, Wan H, Hu T et al (2014) Rapid increase in the risk of extreme summer heat in Eastern China. Nat Clim Chang 4:1082–1085. https://doi.org/10.1038/nclimate2410

Wang Y, Ren F, Zhang X (2014) Spatial and temporal variations of regional high temperature events in China. Int J Climatol 34(10):3054–3065. https://doi.org/10.1002/joc.3893

Wang Q, Liao Z, Zhai P, Peng Y (2024) Record-breaking heatwave in North China during the midsummer of 2023. Int J Climatol 44(12):4206–4218. https://doi.org/10.1002/joc.8577

Wei K, Chen W (2011) An abrupt increase in the summer high temperature extreme days across China in the mid-1990s. Adv Atmos Sci 28:1023–1029. https://doi.org/10.1007/s00376-010-0080-6

Wu LY, Zhang JY (2015) The relationship between spring soil moisture and summer hot extremes over North China. Adv Atmos Sci 32(12):1660–1668. https://doi.org/10.1007/s00376-015-5003-0

Wu X, Wang L, Yao R, Luo M, Li X (2021) Identifying the dominant driving factors of heat waves in the North China Plain. Atmospheric Res 252:105458. https://doi.org/10.1016/j.atmosres.2021.105458

Wu T, Li B, Lian L, Zhu Y, Chen Y (2022) Assessment of the combined risk of drought and high-temperature heat wave events in the North China Plain during summer. Remote Sens 14:4588. https://doi.org/10.3390/rs14184588

Xiao H, Xu P, Wang L (2024) The Unprecedented 2023 North China heatwaves and their S2S predictability. Geophys Res Lett 51:e2023GL107642. https://doi.org/10.1029/2023GL107642

Xu Y, Fang J, Wang P, Qiu X, Tang J (2024) Effect of soil moisture on future heatwaves over eastern China: Convection-permitting regional climate simulations. J Geophys Res: Atmosph 129:e2024JD041654. https://doi.org/10.1029/2024JD041654

Yang Z, Zhang J, Wu L (2019) Spring soil temperature as a predictor of summer heatwaves over Northwestern China. Atmos Sci Lett 20(3):e887. https://doi.org/10.1002/asl.887

Zhang J, Liu ZY, Chen L (2015) Reduced soil moisture contributes to more intense and more frequent heat waves in Northern China. Adv Atmos Sci 32(9):1197–1207. https://doi.org/10.1007/s00376-014-4175-3

Zhang Z, Chen Y, Wang C, Wang P, Tao F (2017) Future extreme temperature and its impact on rice yield in China. Int J Climatol 37:4814–4827. https://doi.org/10.1002/joc.5125

Zhu J, Wang S, Huang G (2016) Assessing climate change impacts on human-perceived temperature extremes and underlying uncertainties. J Geophys Res Atmos 124:3800–3821. https://doi.org/10.1029/2018JD029444